RSC Advances

ROYAL SOCIETY OF CHEMISTRY

PAPER

View Article Online
View Journal | View Issue

Cite this: *RSC Adv.*, 2025, **15**, 13896

Novel phenothiazine-based sensitizers for high-performance dye-sensitized solar cells: enhanced photovoltaic properties through strategic Co-sensitization with N719 †

Sara H. Yousef, Ehab Abdel-Latif, * Safa A. Badawy and Mohamed R. Elmorsy

Received 29th January 2025
Accepted 16th April 2025

DOI: 10.1039/d5ra00694e

rsc.li/rsc-advances

This study presents a systematic investigation of novel phenothiazine-based sensitizers (**SR1–6**) for dye-sensitized solar cells (DSSCs), both as individual sensitizers and in co-sensitization with ruthenium-based **N-719** dye. The compounds exhibited notable spectral properties when adsorbed on TiO_2, demonstrating significant bathochromic shifts and broadened absorption profiles, indicative of strong electronic coupling with the semiconductor surface. Electrochemical characterization confirmed optimal energy level alignment, with ground state oxidation potentials (GSOP) ranging from −5.75 to −6.02 eV and excited state oxidation potentials (ESOP) between −3.54 and −3.77 eV, facilitating efficient electron injection and dye regeneration. In single-dye configurations, **SR1** achieved the highest efficiency of 4.22% with a short-circuit current density (J_{sc}) of 11.96 mA cm^{-2}, while co-sensitization with **N-719** resulted in substantial improvements, particularly for **SR6** + **N-719**, which attained 9.77% efficiency with a J_{sc} of 21.63 mA cm^{-2}. Electrochemical impedance spectroscopy revealed that successful co-sensitized devices exhibited enhanced charge transfer resistance (R_{ct}) values, indicating reduced electron recombination and improved interface stability. This comprehensive study provides valuable insights into molecular design strategies for efficient DSSC sensitizers and demonstrates the efficacy of strategic co-sensitization approaches.

1. Introduction

The escalating global energy demand, coupled with the urgent need to address climate change, underscores the necessity of transitioning from fossil fuels to sustainable energy sources. This challenge is further intensified by population growth and the increasing energy requirements of developing nations. To meet these demands, it is imperative to identify renewable energy solutions that are both cost-efficient and reliant on widely available raw materials. Among the various renewable energy options, solar energy emerges as a particularly promising candidate, offering an abundant and economically viable resource that has long been harnessed by nature to sustain life on Earth. Thus, it seems that the only practical solution to the energy problem on a big scale is to use photovoltaic technologies to harvest the sun's power.[1] The commercialized PV devices initially generated, which used cells made of silicon, had an efficiency of more than 25%. Nevertheless, the extensive usage of these gadgets is limited by their expensive methods.[2] Because of this, Organic Photovoltaics, or OPVs, or Organic Solar Cells, have recently attracted a lot of interest from industry and researchers. In 1991, O'Regan and Graztel invented dye-sensitized solar cells (DSSCs), a new type of photosensitizer that is becoming more and more popular as a viable alternative to high-cost conventional silicon solar cells because of inexpensive material cost, structural tunability, and relatively high performance, as well as simple fabrication process.[3] DSSCs structure consists of a nanocrystalline TiO_2 photoanode, sensitized with metal complexes or metal-free dye molecules to facilitate light harvesting. This photoanode is immersed in an electrolyte containing the I^-/I_3^- redox couple, enabling efficient charge transport and regeneration.[4] In the past two decades, various types of photosensitizers have been developed, including metal-containing complexes (zinc polypyridine and ruthenium porphyrin) and metal-free dyes.[5] The potential of ruthenium and zinc metal complex dyes for use in dye-sensitized solar cells has been the subject of substantial research. The molar extinction coefficients of ruthenium dyes are low, though, and the metal itself is expensive and uncommon. Due to their greater molar extinction coefficients, simple synthesis, and significantly lower cost, as well as the fact that their production requires laborious purifying methods, pure organic dyes have received more attention in the field of

---

Department of Chemistry, Faculty of Science, Mansoura University, Mansoura 35516, Egypt. E-mail: ehabattia00@gmx.net

† Electronic supplementary information (ESI) available. See DOI: https://doi.org/10.1039/d5ra00694e

research and development.[6] Significant advancements have been made in this field, and a number of potential electron donors like triphenylamine, diphenylamine, carbazole, indoline, tetrahydroquinoline, phenoxazine, and phenothiazine have been investigated.[7] Among many kinds of metal-free organic sensitizers, the phenothiazine (PTZ)-based organic dyes have garnered significant scientific attention since their initial investigation by Sun *et al.* in 2007.[8] The introduction of PTZ as a donor in the molecular structure of the sensitizer has resulted in photovoltaic performance that meets acceptable standards. Because of its ground-state non-planar butterfly shape, which reduces aggregation, PTZ donors are an especially promising kind of donor.[9] Moreover, PTZ is a heterocyclic molecule containing a nitrogen atom and an electron-rich sulfur atom in the same six-membered ring, making it an extremely potent electron donor, surpassing the capabilities of triphenylamine, tetrahydroquinoline, carbazole, iminodibenzyles and other *N*-heterocycles.[10] In light of this, we developed and produced a class of chemical dyes (**SR1–6**) in this study that have phenothiazine as a potent donor moiety linked to various acceptor moieties (Fig. 1). Furthermore, the experimental data was verified by theoretical calculations based on density functional theory carried out by Gaussian software. The choice of these six acceptor moieties for phenothiazine-based sensitizers (**SR1–SR6**) was driven by their potential to enhance intramolecular charge transfer (ICT), optimize energy level alignment, and improve light absorption in (DSSCs). These acceptors 4-cyanoacetamide derivatives (**SR1–2**), nitroacetonitrile (**SR3**), pyrazolone (**SR4**), thiazolidinone (**SR5**), and barbituric acid (**SR6**) were carefully selected to explore the effect of different electron-withdrawing groups on DSSC performance.[10,11] Compared to state-of-the-art acceptor units such as cyanoacrylic acid, and pyridine derivatives, these moieties offer stronger electronic coupling with the TiO_2 surface, extended conjugation, and enhanced dye adsorption, all of which are critical for efficient electron injection and reduced charge recombination.[11] Notably, barbituric acid (**SR6**) and thiazolidinone (**SR5**) have been previously explored in different dye backbones, but their integration into phenothiazine-based sensitizers is relatively novel, allowing for enhanced charge separation due to the non-planar butterfly structure of phenothiazine. Similarly, pyrazolone (**SR4**) has been widely utilized in organic electronics, but its potential in DSSCs remains underexplored, making it a promising candidate for improving light absorption while minimizing dye aggregation. The cyanoacetamide (**SR1**) and cyanoacetanilide (**SR2**) groups, on the other hand, are well-known for their strong electron-withdrawing nature, yet their precise influence on DSSC performance when attached to a phenothiazine donor has not been extensively studied. By systematically varying these acceptor moieties, this study provides new insights into structure–property relationships, demonstrating how different electron-withdrawing units impact DSSC efficiency, charge transfer resistance, and spectral absorption. This approach allows for a more rational molecular design strategy compared to traditional DSSC sensitizers, potentially paving the way for higher efficiency, lower recombination losses, and broader light absorption spectra in future dye engineering.

2. Experimental section

2.1. Synthesis

2.1.1. Synthesis of 10-heptyl-10*H*-phenothiazine-3-carbaldehyde (3). 10-Heptyl-10*H*-phenothiazine-3-carbaldehyde (3) has been synthesized through two reactions. Firstly, alkylation reaction between (0.2 g, 1 mmol phenothiazine) and

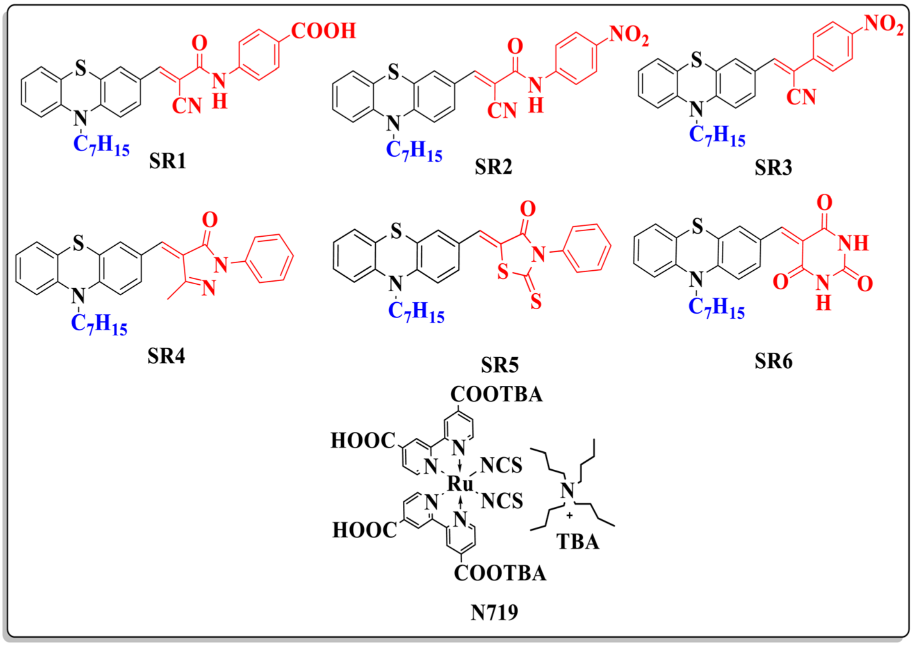

Fig. 1 Molecular structures of sensitizers SR1–6 compared to N719.

(0.3 mL heptyl bromide) with (0.3 g NaH) in presence of DMF, then, stirring for 2 h. Poured into 100 mL ice-cold water and extracted with ethyl acetate. The oily heptyl phenothiazine compound is produced. Subsequently, 2.8 mL (30 mmol) of newly purified $POCl_3$ was added dropwise to a stirred solution of dry DMF (2.75 mL, 35 mmol) at 0 °C under an argon atmosphere until the colored vilsmeier salt fully precipitated. A solution of 10-heptyl-10*H*-phenothiazine (0.3 g, 1 mmol) in 10 mL of DMF was added to the reaction mixture dropwise while continuously stirring for 1 hour. The temperature was elevated to 70 °C, and thereafter, the reaction mixture was stirred overnight. Thereafter, the mixture was placed into 100 mL of ice-cold water and extracted using ethyl acetate. The oily 10-heptyl-10*H*-phenothiazine-3-carbaldehyde product is formed[12] with yield 93%. The specific **SR1–6** sensitizers were produced by means of a Knoevenagel reaction.

2.1.2. General synthesis of sensitizers SR1–6. 10-Heptyl-10*H*-phenothiazine-3-carbaldehyde (**3**) (0.32 g, 1 mmol) was dissolved in 20 mL acetic acid added to 1 mmol of corresponding sensitizer (namely,4-(2-cyanoacetamido)benzoic acid (**4a**), 2-cyano-*N*-(4-nitrophenyl)acetamide (**4b**), 2-(4-nitrophenyl) acetonitrile (**5**), 5-methyl-2-phenyl-2,4-dihydro-3*H*-pyrazol-3-one (**6**), 3-phenyl-2-thioxothiazolidin-4-one (**7**) and pyrimidine-2,4,6 (1*H*,3*H*,5*H*)-trione) (**8**) then (0.1 g, 1 mmol) of sodium acetate in a round-bottomed flask. The flask's contents were heated for 5 hours, then cooled to room temperature, resulting in the formation of a precipitate. Subsequently, the precipitate was purified by recrystallization from ethanol. Fig. from S2 to S25 †showed all the spectral analysis including (IR, ^{1}HNMR, ^{13}CNMR and mass) for compounds **SR1–6**.

2.1.3. 4-(2-Cyano-3-(10-heptyl-10*H*-phenothiazin-3-yl) acrylamido) benzoic acid (SR1). Red crystal (78% yield); m.p. = 230–232 °C. IR (KBr) ν_{max} cm^{-1}: 3330 (N–H), 3014–2834 (C–H aliphatic), 2212 (C≡N), 1675 (C═O). ^{1}H NMR (DMSO-d_6): δ 0.83 (br. s, 3H, CH_3), 1.23 (s, 6H, CH_2), 1.40 (s, 2H, CH_2), 1.71 (s, 2H, CH_2), 3.96 (s, 2H, CH_2), 7.02–7.03 (m, 1H, Ar–H), 7.10 (d, J = 7.20 Hz, 1H, Ar–H), 7.18–7.24 (m, 3H, Ar–H), 7.81 (d, J = 7.20 Hz, 3H, Ar–H), 7.89 (d, J = 7.60, 1H, Ar–H), 7.96 (d, J = 7.20 Hz, 2H, Ar–H), 8.16 (s, 1H, ═CH), 10.57 (s, 1H, N–H), 12.83 (s, 1H, OH) ppm. ^{13}C NMR (DMSO-d_6): δ 14.39, 22.42, 26.43, 26.54, 28.68, 31.68, 47.35, 103.51, 116.27, 116.96, 117.22, 120.19, 122.59, 123.77, 124.10, 126.20, 126.44, 126.49, 127.78, 128.51, 128.99, 130.76 (2C), 131.65, 142.96, 143.26, 149.04, 150.22, 161.77, 167,34 ppm. Mass analysis (*m*/*z*, %): 511 (M$^+$, 31.15), 510 (100.00), 508 (57.35), 340 (76.98), 329 (67.90), 281 (78.93), 138 (48.67), 85 (56.99), 80 (63.67). Analysis for $C_{30}H_{29}N_3O_3S$ (511.64): calculated: C, 70.43; H, 5.71; N, 8.21%. Found: C, 70.54; H, 5.77; N, 8.14%.

2.1.4. 2-Cyano-3-(10-heptyl-10*H*-phenothiazin-3-yl)-*N*-(4-nitrophenyl) acrylamide (SR2). Dark red crystal (74% yield); m.p. = 200–202 °C. IR (KBr) ν_{max} cm^{-1}: 3326 (N–H), 2920–2847 (C–H aliphatic), 2207 (C≡N), 1682 cm^{-1} (C═O) cm^{-1}. ^{1}H NMR (DMSO-d_6): δ 0.79–0.82 (m, 3H, CH_3), 1.21–1.23 (m, 4H, CH_2), 1.25–1.28 (m, 2H, CH_2), 1.36–1.39 (m, 2H, CH_2), 1.67–1.70 (m, 2H, CH_2), 3.94 (t, J = 7.50 Hz, 2H, CH_2), 7.00 (t, J = 8.00 Hz, 1H, Ar–H), 7.08 (d, J = 8.00 Hz, 1H, Ar–H), 7.15–7.24 (m, 3H, Ar–H),7.78 (s, 1H, Ar–H), 7,88 (d, J = 8.50 Hz, 1H, Ar–H), 7.92 (d, J = 8.50 Hz, 2H, Ar–H), 8.169 (s, 1H, ═CH), 8.26 (d, J = 8.50 Hz, 2H, Ar–H), 10.80 (s, 1H, NH) ppm. ^{13}C NMR (DMSO-d_6): δ13.91, 21.94, 25.94 (2C), 28.19, 31.21, 46.90, 102.65, 115.82, 116.54, 116.62, 120.15 (2C), 122.08, 123.30, 123.69, 124.84 (2C), 125.60, 127.32, 128.07, 128.59, 131.37, 142.72, 142.83, 144.68, 148.81, 150.288, 161.69 ppm. Mass analysis (*m*/*z*, %): 512 (M$^+$, 90.73), 488 (53.25), 445 (59.90), 378 (51.65), 351 (77.18), 345 (51.99), 271 (78.35), 201 (100.00), 156 (52.23), 138 (51.41), 136 (57.62), 73 (62.86). Analysis for $C_{29}H_{28}N_4O_3S$ (512.63): calculated: C, 67.95; H, 5.51; N, 10.93%. Found: C, 68.09, H 5.58, N, 10.83%.

2.1.5. 3-(10-Heptyl-10*H*-phenothiazin-3-yl)-2-(4-nitrophenyl) acrylonitrile (SR3). Red solid (62% yield); m.p. = 220–222 °C. IR (KBr) ν_{max} cm^{-1}: 2919–2849 (C–H aliphatic), 2210 (C≡N) cm^{-1};^{1}H NMR (DMSO-d_6): δ 0.83 (t, J = 7.20 Hz, 3H, CH3), 1.23–1.30 (m, 6H, CH_2), 1.38–1.42 (m, 2H,CH_2), 1.68–1.72 (m, 2H, CH_2), 3.94 (t, J = 6.80 Hz, 2H, CH_2), 7.01 (t, J = 7.60 Hz, 1H, Ar–H), 7.08 (d, J = 8.40 Hz, 1H, Ar–H), 7.17–7.20 (m,2H, Ar–H), 7.24 (t, J = 8.00 Hz, 1H, Ar–H), 7.80 (s, 1H, Ar–H), 7.90 (d, J = 8.80 Hz, 1H, Ar–H), 7.99 (d, J = 8.80 Hz, 2H, Ar–H), 8.15 (s, 1H, ═CH), 8.34 (d, J = 8.80 Hz, 2H, Ar–H) ppm. ^{13}C NMR (DMSO-d_6): δ 14.39, 22.42, 26.44, 26.55, 28.68, 31.69, 47.26, 105.22, 116.21, 116.32, 118.32, 122.64, 123.71, 123.89, 124.82 (2C), 126.96 (2C), 127.75 (2C), 128.46, 128.52, 130.65, 141.01, 143.54, 145.22, 147.40, 147.99 ppm. Mass analysis (*m*/*z*, %): 470 (M$^+$, 4.96), 449 (69.55), 423 (94.87), 418 (69.19), 400 (60.76), 394 (93.99), 379 (77.00), 370 (68.15), 369 (86.19), 366 (68.38), 336 (80.88), 324 (90.89), 170 (100.00), 129 (67.43), 109 (70.09), 74 (60.35). Analysis for $C_{28}H_{27}N_3O_2S$ (469.60): calculated: C, 71.62; H, 5.80; N, 8.95%. Found: C, 71.73; H, 5.75; N, 9.01%.

2.1.6. 4-((10-Heptyl-10*H*-phenothiazin-3-yl)methylene)-5-methyl-2-phenyl-2,4-dihydro-3*H*-pyrazol-3-one (SR4). Reddish black crystal (66% yield); m.p. = 184–186 °C. IR (KBr) ν_{max} cm^{-1}: 2920, 2848 (C–H aliphatic), 1677 (C═O) cm^{-1}. ^{1}H NMR (DMSO-d_6): δ 0.78 (t, J = 7.00 Hz, 3H, CH_3), 1.18–1.25 (m, 6H, CH_2),1.30–1.34 (m, 2H, CH_2), 1.60–1.64 (m, 2H, CH_2), 2.30 (s, 3H, CH_3-pyrazolone), 3.78 (t, J = 6.00 Hz, 2H, CH_2), 6.87–6.91 (m, 2H, Ar–H), 6.95–7.00 (m, 2H, Ar–H),7.07 (t, J = 9.50 Hz, 2H, Ar–H), 7.14–7.18 (m, 1H, Ar–H), 7.19–7.23 (m, 2H, Ar–H), 7.38–7.47 (m, 2H, 1H, ═CH, Ar–H),7.68 (d, J = 8.00 Hz, 2H, Ar–H). ^{13}C NMR (DMSO-d_6): δ 11.86, 13.94, 22.00, 26.21, 28.33, 31.26, 32.58, 46.35, 115.37, 115.54, 116.68, 118.31, 120.31 (2C), 122.20, 122.94, 125.21, 125.76, 126.49, 127.10, 127.56, 128.86 (3C), 137.20, 137.85, 142.74, 144.87, 146.11, 161.93 ppm. Mass analysis (*m*/*z*, %): 481 (M$^+$, 59.09), 393 (68.73), 382 (66.64), 347 (57.04), 344 (60.16), 321 (100.00), 317 (79.69), 278 (77.81), 238 (61.54), 183 (53.42), 154 (65.69). Analysis for $C_{30}H_{31}N_3OS$ (481.66): calculated: C, 74.81; H, 6.49; N, 8.72%. Found: C, 74.64, H, 6.55, N, 8.78%.

2.1.7. 5-((10-Heptyl-10*H*-phenothiazin-3-yl) methylene)-3-phenyl-2-thioxothiazolidin-4-one (SR5). Dark red crystal (64% yield); m.p. = 130–132 °C. IR (KBr) ν_{max} cm^{-1}: 2954–2851 (C–H aliphatic), 1704 (C═O) cm^{-1}. ^{1}H NMR (DMSO-d_6): δ 0.03 (t, J = 7.00 Hz, 3H, CH_3), 0.37–0.42 (m, 6H, CH_2), 0.52–0.54 (m, 2H, CH_2), 0.83–0.85 (m, 2H, CH_2), 3.07 (t, J = 6.50 Hz, 2H, CH_2), 6.14 (t, J = 7.50 Hz, 1H, Ar–H), 6.22 (d, J = 8.00 Hz, 1H, Ar–H),6.32 (t, J = 6.50 Hz, 2H, Ar–H),6.37 (t, J = 7.50 Hz, 1H, Ar–H), 6.54 (d, J = 8.00 Hz, 2H, Ar–H), 6.58 (s, 1H, Ar–H), 6.64–6.67 (m, 2H, Ar–H), 6.69–6.71 (m, 2H, Ar–H),6.87 (s, 1H, =CH) ppm. ^{13}C NMR (DMSO-d_6): δ 14.40, 22.43, 26.47, 26.58, 28.69, 31.69, 47.32, 116.70, 116.87, 120.57, 122.73, 123.93, 124.39, 127.68, 127.77, 128.47, 129.25 (2C), 129.80 (2C), 129.90 (2C), 131.11, 132.39, 135.80, 143.54, 147.51, 167.44, 193.93 ppm. Mass analysis (*m*/*z*, %): 516 (M$^+$, 14.96), 407 (36.51), 366 (34.28), 335 (100.00), 264 (47.92), 226 (41.87), 145 (41.82). Analysis for $C_{29}H_{28}N_2OS_3$ (516.74): calculated: C, 67.41; H, 5.46; N, 5.42%. Found: C, 67.54; H, 5.52; N, 5.37%.

2.1.8. 5-((10-Heptyl-10*H*-phenothiazin-3-yl) methylene) pyrimidine-2,4,6(1*H*,3*H*,5*H*)-trione (SR6). Reddish brown solid (74% yield); m.p. > 300 °C. IR (KBr) ν_{max} cm^{-1}: 2924–2850 (C–H aliphatic), 1719 (C=O) cm^{-1}. ^{1}H NMR (DMSO-d_6): δ 0.81–0.83 (m, 3H, CH$_3$), 1.23–1.36 (m, 8H, CH$_2$), 1.62–1.73 (m, 2H, CH$_2$), 3.78–3.88 (m, 2H, CH$_2$), 5.83 (s, 1H, =CH), 6.71 (s, 1H, Ar–H), 6.84 (s, 2H, Ar–H), 6.89 (t, J = 7.20 Hz, 1H, Ar–H), 6.96 (d, J = 8.40 Hz, 1H, Ar–H), 7.10 (d, J = 7.20 Hz, 1H, Ar–H), 7.17 (t, J = 7.60 Hz, 1H, Ar–H), 10.08 (s, 2H, N–H). ^{13}C NMR (DMSO-d_6): δ 14.40, 21.63, 22.45, 26.70, 28.78, 31.71, 46.80, 91.25, 115.46, 115.82, 122.39, 122.60, 123.99, 125.60, 126.45, 127.49, 127.86, 139.63, 142.03, 145.61, 151.13 (2C), 172.59 (2C) ppm. Mass analysis (*m*/*z*, %): 435 (M$^+$, 30.70), 430 (100.00), 376 (76.30), 368 (57.06), 357 (55.41), 351 (62.58), 331 (66.16), 294 (57.18), 280 (60.32), 178 (97.02), 174 (80.85), 133 (54.97), 115 (70.95), 87 (75.61), 86 (87.65). Analysis for $C_{24}H_{25}N_3O_3S$ (435.54): C, 66.19; H, 5.79; N, 9.65%. Found: C, 66.33; H, 5.85; N, 9.74%.

3. Results and discussion

3.1. Chemistry

The synthetic routes of the new phenothiazine based organic sensitizers (**SR1–6**) are depicted in Scheme 1. First, the alkylation reaction between 10*H* phenothiazine (**1**) using heptyl bromide with NaH in presence of DMF afforded 10-heptyl-10*H*-phenothiazine (**2**), which undergoes Vilsmeier formylation using POCl$_3$ in DMF to yield 10-heptyl-10*H*-phenothiazine-3-carbaldehy (**3**) with a good overall yield.

1-Cyanoacetyl-3,5-dimethylpyrazole has been utilized as an effective reagent for cyanoacetylation of different primary aromatic amines such as 4-nitroaniline and 4-aminobenzoic acid to furnish the conforming cyanoacetanilide **4a–b** as previously described in the literature.[13] Next, the Knoevenagel reaction between cyanoacetanilides **1a–b** and 10-heptyl-10*H*-phenothiazine-3-carbaldehyde (**3**) in acetic acid in presence of sodium acetate to afford cyanoacetanilide sensitizers **SR1–2** (Scheme 1). The other four new organic sensitizers **SR3–6** were obtained by Knoevenagel condensation wherein the 10-heptyl-10*H*-phenothiazine-3-carbaldehyde (**3**) was condensed with different active methylene compounds such as 2-(4-nitrophenyl) acetonitrile (**5**), 5-methyl-2-phenyl-2,4-dihydro-3*H*-pyrazol-3-one (**6**), 3-phenyl-2-thioxothiazolidin-4-one (**7**) and pyrimidine-2,4,6(1*H*,3*H*,5*H*)-trione (**8**) as shown in Scheme 1.

3.2. UV-vis absorption and electrochemical properties

The UV-vis absorption spectra of the synthesized phenothiazine sensitizers **SR1–6** were analyzed as presented in Table 1. The absorption spectra of **SR1–6** have been recorded in DMF solution and are shown in Fig. 2.

The dyes **SR1–6** exhibited two distinct absorption regions, one at shorter wavelengths (250–400 nm) and another at longer wavelengths (420–600 nm). The shorter-wavelength bands were attributed to π–π* electronic transitions, indicative of the conjugated nature of the systems. In contrast, the absorption

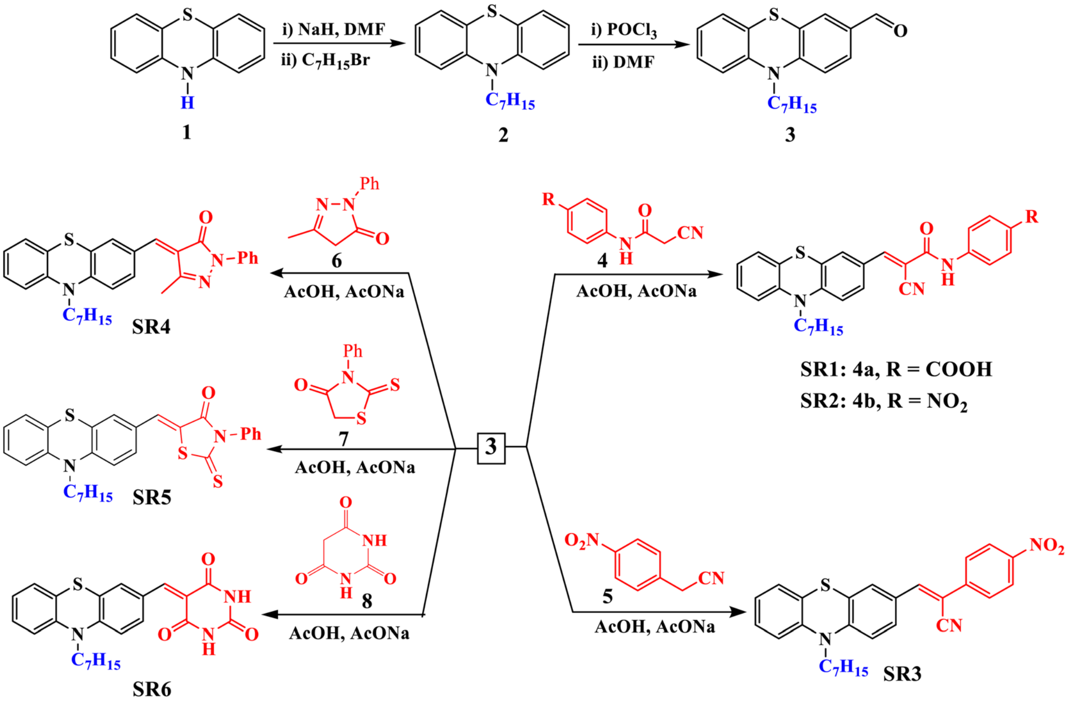

Scheme 1 Synthesis of compound 3 and sensitizers SR1–6.

Table 1 Absorption for phenothiazine sensitizers **SR1–6**

Sensitizer	λ_{max}/nm	$\varepsilon/10^4\ M^{-1}\ cm^{-1}$	λ_{onset}/nm	Experimental E_{0-0} (eV)
SR1	319, 447	4.48, 2.75	544	2.27
SR2	322, 460	2.98, 2.62	563	2.20
SR3	327, 452	4.06, 2.52	549	2.25
SR4	300, 526	1.30, 3.91	617	2.00
SR5	357, 470	1.98, 2.49	566	2.19
SR6	300, 490	2.28, 3.03	608	2.03

features in the visible range (420–600 nm) were ascribed to intramolecular charge transfer (ICT) processes between the phenothiazine donor and various acceptor groups, including CN, CO, COOH, and NO_2.[14] Specifically, ICT transitions were observed in the 2-cyanacetamide derivatives (CN and NO_2) of the 2-(4-nitrophenyl) acrylonitrile unit for **SR3**, the (CO) group within the pyrazol-3-one ring for **SR4**, the (CN and CS) groups in the thiazolidin-4-one ring for **SR5**, and the (3 CO) groups in the barbituric ring. The incorporation of a π-bridge was found to enhance light absorption in the visible region, effectively reducing energy gap (E_{0-0}), as calculated from the onset of the UV-visible absorption spectrum.[14] Those values followed the order of **SR4** < **SR6** < **SR5** < **SR2** < **SR3** < **SR1**. The molar extinction coefficients (ε) of the ICT bands of **SR1–6** are (2.75, 2.62, 2.52, 3.91, 2.49, and 3.03 × 10^4 mol^{-1} cm^{-1}, respectively). The values of the molar extinction coefficient (ε) are significantly greater than those of the Ru dyes **N719** ($\varepsilon = 1.08 \times 10^4$ M^{-1} cm^{1}), indicating a strong capacity for light-harvesting.[15] Increasing the difference in electronic density between the donating and withdrawing electrons induces a bathochromic shift in the internal charge transfer (ICT) band.[16] A strong electron-accepting group, on the other hand, should improve the dye's push–pull character and facilitate charge separation within the molecule.[17] Also, sensitizers, **SR4**, and **SR6** showed significantly greater, red-shifted profiles than **SR5**. This shift can be attributed to the extended conjugation length within the molecule.[18] Furthermore, **SR4** absorbs at the highest wavelength λ_{max} equal to 526 nm at a high value of ε at 3.91 × 10^{-4} M^{-1} cm^{-1} which can be explained by the reduced electron delocalization energy of the electron-acceptors and by the presence of five-atom structures (methyl pyrazole), which are smaller in size than the six-member ring.[19]

When absorbed onto nonporous TiO_2, the absorption spectra of dyes **SR1–6** undergo significant alterations compared to their solution-phase counterparts, illuminating the fundamental interactions between the dyes and the semiconductor surface (Fig. 3). All compounds exhibit pronounced spectral broadening and bathochromic shifts; phenomena attributed to several fundamental photophysical processes. The strong electronic coupling between the carboxylate anchor groups and the TiO_2 surface leads to efficient orbital mixing, as previously demonstrated by Chen *et al.*[20] and further supported by recent spectroscopic studies.[21] This coupling is particularly evident in **SR1** and **SR6**, where the direct connection between the donor and anchor groups facilitates strong electronic interaction with the semiconductor surface. The observed spectral broadening is enhanced by the formation of *J*-aggregates on the TiO_2 surface, a phenomenon well-documented for similar donor-π-acceptor systems.[22,23] The non-planar butterfly structure of the phenothiazine core plays a crucial role in determining the electronic properties of these sensitize.[24,25] In solution, the absorption spectra of **SR1–SR6** exhibit distinct variations, which can be attributed to intramolecular charge transfer (ICT) transitions, influenced by the nature of donor–acceptor interactions and solvent effects. However, when adsorbed on TiO_2, most of the sensitizers display similar spectral features, except for **SR4**, which remains almost unshifted. Sensitizers **SR1**, **SR2**, **SR3**, **SR5**, and **SR6** possess highly conjugated acceptor groups (COOH, CN, CS, or barbituric rings) that facilitate stronger charge transfer interactions upon adsorption. **SR4**, however, contains a pyrazolone ring, which may alter its adsorption geometry, reducing direct electronic overlap with TiO_2 and thus minimizing shifts in its absorption spectrum. The observed

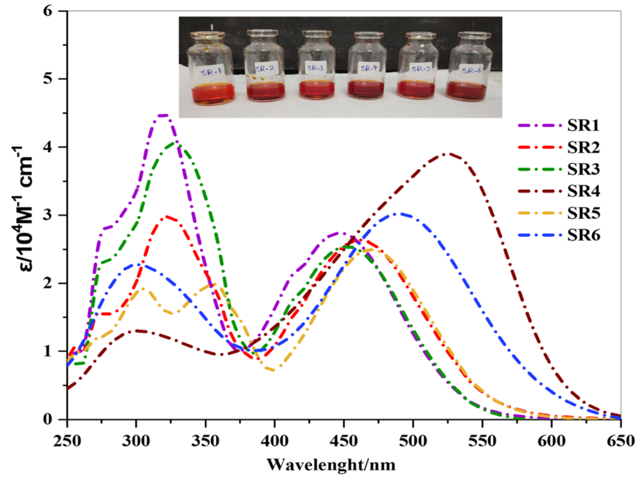

Fig. 2 UV-vis absorption spectra of PTZ sensitizers **SR1–6** measured in DMF.

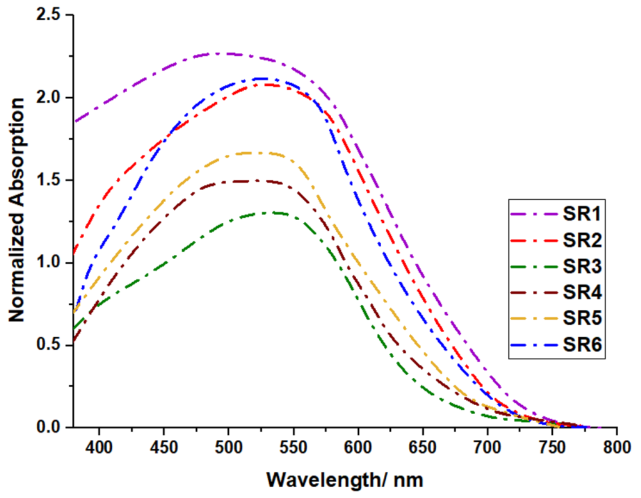

Fig. 3 Absorption spectra of **SR1–6** adsorbed on nonporous TiO_2.

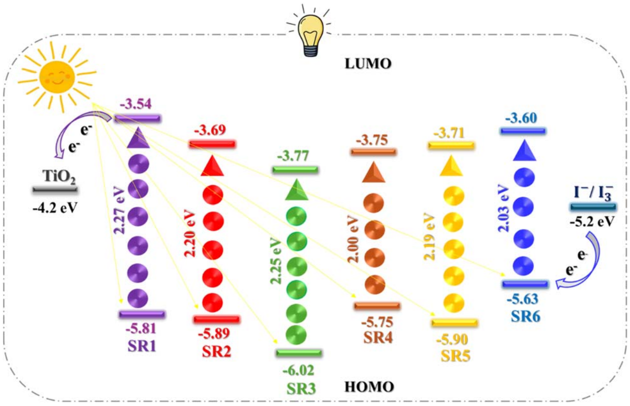

Fig. 4 Energy level diagram for **SR1–6** sensitizers.

spectral similarities upon TiO$_2$ adsorption, aside from **SR4**, can be attributed to strong electronic coupling, *J*-aggregation effects, and charge transfer interactions, leading to spectral broadening and red shifts. The unique behavior of **SR4** suggests that its molecular structure restricts significant interaction with TiO$_2$, preserving its solution-phase absorption properties.

To assess the potential for dye regeneration and electron injection, cyclic voltammetry (CV) experiments were performed in THF with TBAPF$_6$ as the supporting electrolyte, as illustrated in Fig. (S26†). The results, summarized in Table (S1†), reveal that the energy levels of the dyes are well-aligned for efficient operation in dye-sensitized solar cells (DSSCs). The ground-state oxidation potentials (GSOP) of the compounds, spanning from −5.75 to −6.02 eV, are significantly more negative than the I^-/I_3^- redox couple (−5.2 eV), ensuring an adequate driving force for effective dye regeneration.[26,27] The excited state oxidation potentials (ESOP), calculated from GSOP levels and E_{0-0} values, range from −3.54 to −3.77 eV, positioning them favorably above the TiO$_2$ conduction band (−4.2 eV). This energy level alignment provides adequate driving force for electron injection, as demonstrated by Zhang and coworkers in related systems as shown in (Fig. 4).[28,29] The experimental values show excellent agreement with theoretical calculations, validating our molecular design strategy and energy level engineering approach.[30]

3.3. Theoretical calculations

3.3.1. Molecular modeling. The **SR1–6** sensitizers were subjected to density-functional theory (DFT) calculations utilizing the B3LYP with the d-polarized 6-311G basis that is implemented in the Gaussian09 program.[31] As shown in Fig. S27,† the optimized structure for compounds **SR1–6**, and elucidate the relationship between the six **SR1–6** sensitizer dyes' geometric structure and Fig. 5 and6 the electrical distribution of their HOMO and LUMO levels in additional detail. For the **SR1** sensitizer, the HOMO electron density was mostly localized on the donor parts (phenothiazine ring), while electronic densities of LUMO were mostly localized on CN, CO, and COOH segments. But in the case of **SR2**, the electron density of LUMO extended towards the acceptor moieties (CN, CO, and NO$_2$). Also, the HOMO of **SR3** was mostly concentrated in the donor parts (phenothiazine ring), while the 4-nitroacetonitrile acceptor moiety (CN and NO$_2$) was where the majority of the LUMO electron density was located. For **SR5** introduction thiazolidine-4-one ring facilitates the transfer of electrons from the phenothiazine moiety's donor side to its acceptor side that is centered on the (C=S and carbonyl) segments. In the case of **SR6**, the barbituric acid anchoring part possesses the LUMO electron density.

3.3.2. Molecular electrostatic potential (MEP). From the cube file produced by Gaussian computations, molecular electrostatic potentials (MEPs) can be extracted as a useful tool for identifying organic molecule internal charge transfer (ICT) properties, in this case between the HOMO and LUMO levels of phenothiazine in **SR1–6** dyes.[32] Fig. 7 shows the results of analyzing the HOMO–LUMO levels and MEPS of all **SR1–6**

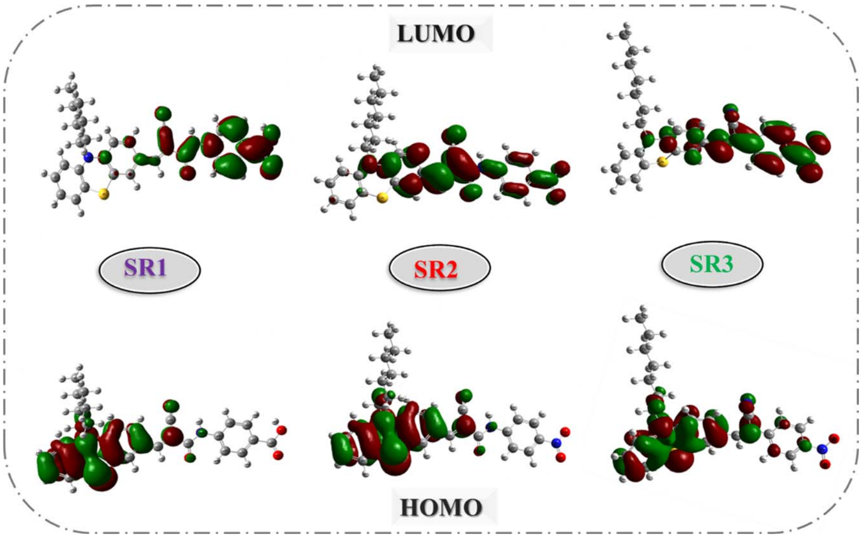

Fig. 5 HOMOs and LUMOs geometry for **SR1–2**.

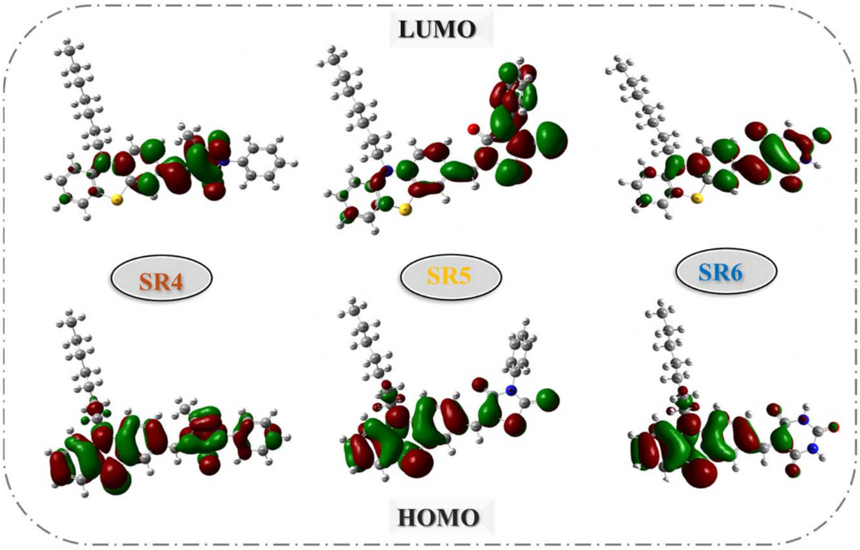

Fig. 6 HOMOs and LUMOs geometry for **SR3–6**.

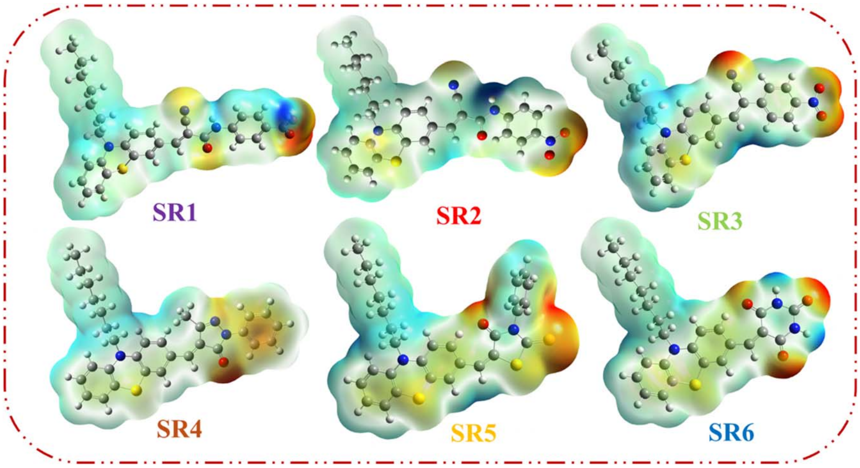

Fig. 7 Molecular electronic potential diagram (MEP) of sensitizers **SR1–6**.

sensitizers to determine the impact of donor–acceptor groups. Electrophilic activity is found in the red parts of the MEP, which are related to electron-rich regions, while nucleophilic activity is found in the blue parts, which are associated with electron-deficient portions of sensitizers **SR1–6**. Electrostatic potential increased in the following order: red, orange, yellow, green, and blue. For the **SR1** sensitizer, which incorporates a cyanoacetamide moiety, the negative (red) charge is primarily localized on the cyano group and the carbonyl group connected to the COOH moiety. In **SR2**, the negative (red) low potential is predominantly concentrated in the region of the anchoring group, specifically within the cyano, carbonyl, and nitro groups. Similarly, in **SR3**, the negative (red) low potential is mainly observed around the anchoring group, with a particular focus on the cyano (CN) and nitro (NO_2) groups. In contrast, for **SR4**, the pyrazole ring's carbonyl (CO) group is identified as the main site of the negative charge. The carbonyl group on the thiazolidine-4-one ring and the C=S group are the specific locations where the red color is concentrated for the **SR5** sensitizer. Finally, **SR6,** the negative (red) low potentials concentrated on the carbonyl groups of the barbituric ring. The positive region (blue) of the MEP map is found across the donor heptyl phenothiazine region, indicating that they are favorable sites for nucleophilic attack.

3.4. Photovoltaic performance for sensitizers SR1–6

The photovoltaic properties of phenothiazine sensitizers **SR1–6** were systematically evaluated under standard conditions using AM 1.5 G. The current density–voltage (*J*–*V*) characteristics are illustrated in Fig. 8, with the detailed performance parameters summarized in Table 2. Dye loading experiments are commonly used to better realize the effect of several anchors on dye performance. Considering this, a DMF/H_2O (1 : 1) combination containing 0.1 M NaOH was used to desorb dye from the TiO_2 surface to quantify the total quantity of dye adsorbed on the TiO_2.

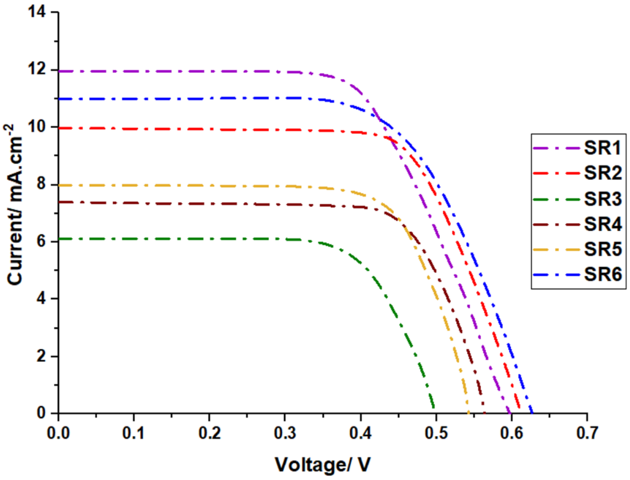

Fig. 8 *I*–*V* characteristics of solar devices based on **SR1–6**.

The photovoltaic parameters of single-dye devices reveal complex structure–performance relationships that provide valuable insights into molecular design principles. **SR1** achieves the highest efficiency (4.22%) among the series, characterized by a short-circuit current density (J_{sc}) of 11.96 mA cm^{-2}, open-circuit voltage (V_{oc}) of 0.597 V, and fill factor (FF) of 59.2%. This superior performance stems from optimal energy level alignment and efficient charge injection dynamics.[33,34] The direct connection between the donor and anchor groups in **SR1** facilitates rapid electron injection into the TiO$_2$ conduction band while maintaining sufficient driving force for dye regeneration.[35] **SR3** exhibits the lowest efficiency (1.83%) with significantly reduced photovoltaic parameters (J_{sc} = 6.08 mA cm^{-2}, V_{oc} = 0.499 V, FF = 60.4%). The poor performance is attributed to the weak anchoring ability of the nitroacetonitrile acceptor moiety, which limits effective electron injection and interfacial interaction with TiO$_2$.[36] The reduced V_{oc} indicates increased charge recombination rates, likely due to the formation of surface trap states at the TiO$_2$/dye interface.[37] Among the single-dye devices, **SR1** exhibited the highest efficiency (4.22%), followed by **SR6** (3.88%), due to their optimal donor-π-acceptor interactions, favorable energy level alignment, and strong charge injection capabilities and the strength of the acceptors moieties, while **SR3** performed the lowest (1.83%), likely due to its weak nitroacetonitrile acceptor, which hinders effective electron injection and increases recombination losses and the lower dye loading of the dye. Sensitizers **SR2** (3.48%), **SR4** (2.64%), and **SR5** (2.51%) showed moderate efficiencies, demonstrating that molecular structures with better anchoring ability and charge transfer dynamics tend to enhance performance, the photovoltaic performance agree with the absorbance of TiO$_2$.

The cocktail co-sensitization strategy with **N719** demonstrates remarkable enhancement in device performance through complementary absorption and reduced aggregation effects. The **SR6** + **N719** system achieves an unprecedented efficiency of 9.77%, characterized by significantly improved photovoltaic parameters (J_{sc} = 21.63 mA cm^{-2}, V_{oc} = 0.743 V, FF = 60.8%). This exceptional performance represents a 33.3% improvement over standard **N719** devices (η = 7.33%) and can be attributed to several synergistic effects[38,39] as shown in Table 3 and Fig. 9.

The variation in cocktail co-sensitization efficiency among **SR** dyes can be directly linked to their molecular structures and resulting electronic properties. **SR6** exhibits optimal GSOP (−5.75 eV) and ESOP (−3.75 eV) levels, positioning it ideally relative to the TiO$_2$ conduction band (−4.2 eV) and the electrolyte redox potential (−5.2 eV).[3,4] This energy level alignment facilitates efficient electron injection into TiO$_2$ while maintaining robust dye regeneration capabilities. The broad absorption spectrum of **SR6** on TiO$_2$, complementing N719's absorption profile, enables enhanced light harvesting across the visible spectrum.[40,41] As shown in Fig. 9, **SR1** and **SR5**, showing similarly impressive co-sensitization performance (η = 8.52% and 7.45% respectively), demonstrate comparable electronic characteristics. Their GSOP values (−5.81 eV and −5.90 eV) and ESOP levels (−3.54 eV and −3.71 eV) create favorable energy cascades for electron injection and dye regeneration.[42] The broadening and red-shifting of absorption spectra observed when SR dyes are adsorbed on TiO$_2$ indicates strong electronic coupling between the dye molecules and the semiconductor surface. This phenomenon is particularly pronounced in **SR6**, **SR1**, and **SR5**, where the extended π-conjugation systems facilitate better electronic communication with both TiO$_2$ and **N719**.[43,44] The lower performance of **SR3** + **N719** (η = 5.70%) correlates with its less favorable GSOP (−6.02 eV) and ESOP (−3.77 eV) levels, resulting in suboptimal electron injection dynamics.[10,11] This is reflected in its lower R_{ct} value (41.52 Ω) as shown in the EIS studies and reduced photovoltaic parameters

Table 2 Photovoltaic parameters of compounds **SR1–6**. Significance values are in bold

Sensitizers	$J_{SC}{}^a$ ($J_{SC}{}^b$) (mA cm^{-2})	$V_{OC}{}^a$ ($V_{OC}{}^b$)/mV	FF^a (FF^b)/%	PCE^a (PCE^b)/%	Concentration of the dye/10^{-5} mol cm^{-2}
SR1	**11.96 (11.88 ± 0.168)**	**0.597 (0.594 ± 0.005)**	**59.20 (59.43 ± 1.69)**	**4.22 (4.21 ± 0.031)**	**0.93**
SR2	**9.95 (9.92 ± 0.046)**	**0.611 (0.602 ± 0.017)**	**57.30 (58.033 ± 1.97)**	**3.48 (3.47±0.052)**	**0.80**
SR3	**6.08 (6.02 ± 0.105)**	**0.499 (0.496 ± 0.005)**	**60.40 (61.053 ± 1.18)**	**1.83 (1.816 ± 0.031)**	0.67
SR4	**7.98 (7.94 ± 0.056)**	**0.563 (0.562 ± 0.005)**	**58.9 (58.58 ± 0.955)**	**2.64 (2.623 ± 0.0318)**	**0.55**
SR5	**7.40 (7.37±0.052)**	**0.543 (0.540 ± 0.005)**	**62.5 (63.2 ± 1.153)**	**2.51 (2.513 ± 0.046)**	**0.50**
SR6	**10.99 (10.96 ± 0.055)**	**0.626 (0.623 ± 0.006)**	**56.4 (56.05 ± 0.551)**	**3.88 (3.88 ± 0.041)**	**0.89**

[a] The best device parameters (listed in the manuscript). [b] The average device parameters (obtained from three devices).

Table 3 Photovoltaic parameters of the **SR1–6** + **N-719** and **N-719** only. Significance values are in bold

Cell device	$J_{SC}{}^a$ ($J_{SC}{}^b$) (mA cm^{-2})	$V_{OC}{}^a$ ($V_{OC}{}^b$)/mV	FF^a (FF^b)/%	PCE^a(PCE^b)/%	Concentration of the dye/10^{-5} mol cm^{-2}
SR1 + **N-719**	**20.53** (**20.55 ± 0.066**)	**0.709** (**0.714 ± 0.012**)	**58.6** (**58.28 ± 0.649**)	**8.52** (**8.56 ± 0.193**)	**2.52**
SR2 + **N-719**	**19.70** (**19.70 ± 0.129**)	**0.637** (**0.637 ± 0.016**)	**56.9** (**56.89 ± 0.188**)	**7.14** (**7.146 ± 0.147**)	**1.65**
SR3 + **N-719**	**16.19** (**16.27 ± 0.142**)	**0.609** (**0.617 ± 0.026**)	**57.90** (**57.96 ± 0.284**)	**5.70** (**5.69 ± 0.115**)	**1.44**
SR4 + **N-719**	**16.93** (**16.89 ± 0.095**)	**0.626** (**0.635 ± 0.019**)	**58.70** (**58.69 ± 0.198**)	**6.22** (**6.20 ± 0.036**)	**1.65**
SR5 + **N-719**	**18.23** (**18.18 ± 0.118**)	**0.680** (**0.685 ± 0.011**)	**60.10** (**60.27 ± 0.402**)	**7.45** (**7.53 ± 0.228**)	**1.77**
SR6 + **N-719**	**21.63** (**21.56 ± 0.474**)	**0.743** (**0.744 ± 0.006**)	**60.80** (**60.82 ± 0.717**)	**9.77** (**9.70 ± 0.126**)	**2.54**
N-719	**19.07** (**19.11 ± 0.220**)	**0.660** (**0.662 ± 0.006**)	**58.30** (**58.163 ± 0.344**)	**7.33** (**7.47 ± 0.374**)	**1.87**

[a] The best device parameters (listed in the manuscript). [b] The average device parameters (obtained from three devices).

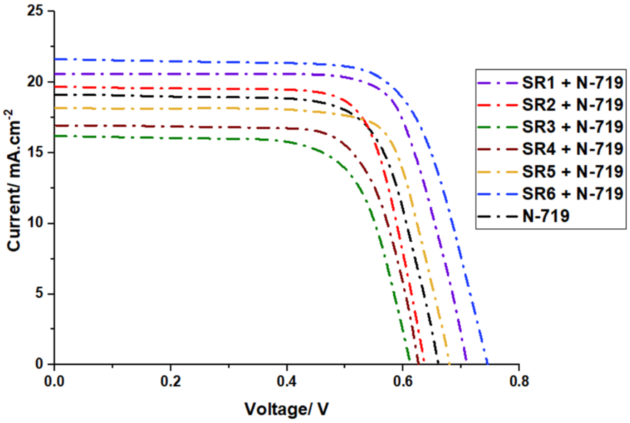

Fig. 9 I–V characteristics of solar devices sensitized with **N-719** and **SR1–6**.

(J_{sc} = 16.19 mA cm^{-2}, V_{oc} = 0.609 V).[45] The underperformance of **SR2–4** in cocktail co-sensitization can be attributed to less favorable molecular arrangements and electronic coupling, resulting in increased charge recombination (lower R_{ct} values) and reduced light harvesting efficiency.[46] Upon co-sensitization with **N719**, the overall efficiencies significantly improved, with **SR6** + **N719** achieving the highest performance (9.77%), followed by **SR1** + **N719** (8.52%) and **SR5** + **N719** (7.45%), attributed to their complementary light absorption, enhanced charge separation, and reduced recombination, as indicated by their higher charge transfer resistance (R_{ct}) values from electrochemical impedance spectroscopy (EIS) studies. Conversely, **SR3** + **N719** exhibited the lowest efficiency (5.70%), reaffirming its poor electron injection dynamics and higher charge recombination rates, while **SR2** + **N719** (7.14%) and **SR4** + **N719** (6.22%) displayed moderate enhancements. The photovoltaic trends directly correlate with their molecular structures, where dyes with extended conjugation, stronger anchoring groups, and optimized energy level alignment consistently outperformed others. Additionally, higher R_{ct} values in co-sensitized devices (**SR6** + **N719:** 49.98 Ω, **SR1** + **N719:** 48.17 Ω) indicate suppressed electron recombination, leading to improved (V_{oc}) and overall efficiency. The comprehensive analysis highlights that efficient co-sensitization relies on synergistic energy level alignment, complementary spectral absorption, and minimized recombination losses, providing valuable insights for the rational design of next-generation DSSC sensitizers with enhanced light-harvesting and charge transport properties.

The incident photon-to-current efficiency (IPCE) spectra of the phenothiazine-based sensitizers **SR1–6** revealed significant differences in their light-harvesting and electron injection efficiencies as shown in Fig. 10.[46] The single-dye DSSCs exhibited broad photoresponse in the 300–600 nm range, with IPCE maxima aligning with their UV-vis absorption peaks. Among them, **SR1** displayed the highest IPCE values (56% at 500 nm), indicating strong light absorption and efficient charge injection into TiO$_2$. In contrast, **SR3** exhibited the lowest IPCE (40%), likely due to its weaker electron-withdrawing acceptor, leading to inefficient charge transfer and increased recombination. The IPCE integral areas of DSSCs exhibit an order for dyes of **SR1** > **SR6** > **SR2** > **SR5** > **SR4** > **SR3**, which is consistent with the trend of J_{SC}.

Upon co-sensitization with **N719**, the IPCE spectra showed a substantial increase, particularly in the 450–600 nm range, confirming improved spectral utilization and enhanced photocurrent generation as shown in Fig. 11. Notably, the **SR6** + **N719** system achieved the highest IPCE (~85% at 500 nm), reflecting superior light absorption, efficient charge injection, and reduced recombination losses. The enhanced IPCE response in

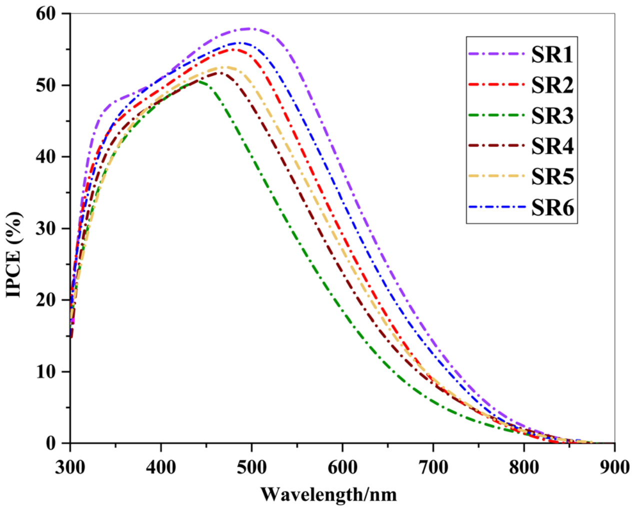

Fig. 10 IPCE spectra of phenothiazine-sensitizer **SR1–6**.

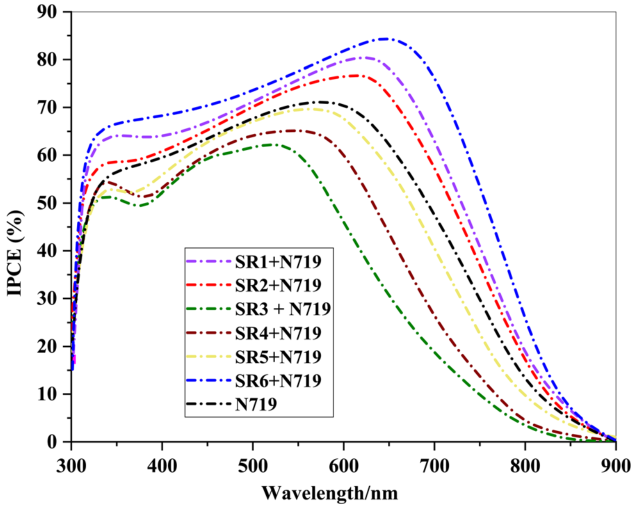

Fig. 11 IPCE spectra of phenothiazine-sensitizer **SR1–6** + **N719** and **N719**.

co-sensitized devices is consistent with their higher (J_{sc}) and (R_{ct}), as confirmed by (EIS), which indicates suppressed recombination and improved electron transport. These results emphasize the importance of co-sensitization in broadening the absorption spectrum, enhancing charge separation, and boosting overall DSSC efficiency.

3.5. Charge transfer dynamics

To further investigate the mechanisms of charge recombination in DSSC configurations, electrochemical impedance spectroscopy (EIS) was performed under a forward bias of 0.70 V in the absence of illumination.[47–50] The Nyquist plots, presented in Fig. 12, display two characteristic semicircles. The smaller semicircle observed in the high-frequency region corresponds to the charge-transfer impedance (R_{Pt}) at the Pt counter electrode, while the larger semicircle in the intermediate-frequency range represents the charge-transfer resistance R_{ct} at the TiO_2/sensitizer/electrolyte interface. An increased R_{ct} value indicates reduced electron recombination, which contributes to an enhancement in the open-circuit voltage (V_{OC}). Additionally, *Rs* represents the series resistance. The values of R_{Pt}, R_{ct}, and R_s were determined by fitting the experimental data to an equivalent circuit model, as shown in the inset of Fig. 11.[51] All DSSC devices exhibited comparable R_s and R_{Pt} values, reflecting the consistent use of identical FTO substrates and Pt electrodes. However, R_{ct} values varied across the devices, following the order: **SR6** + **N-719** (49.98 Ω) > **SR1** + **N-719** (48.17 Ω) > **SR5** + **N-719** (47.22 Ω) > **N-719** (46.08 Ω) > **SR2** + **N-719** (44.56 Ω) > **SR4** + **N-719** (43.24 Ω) > **SR3** + **N-719** (41.52 Ω). This trend is consistent with the observed variations in V_{OC}, as summarized in Table 3. Notably, the co-sensitized devices (**SR6**, **SR1**, and **SR5**) demonstrated higher R_{ct} values compared to devices employing **N-719** alone, indicating a suppression of electron recombination between injected electrons and the electrolyte. This behavior is likely attributed to the formation of a more compact and organized monolayer of sensitizers, facilitated by enhanced dye adsorption.[52,53] Also the Nyquist plots for sensitizers **SR1–6** presented in Fig. (S28),† it observed that R_{ct} values varied across the devices, following the order: **SR6** > **SR2** > **SR1** > **SR4** > **SR5** > **SR3**. This trend is consistent with the observed variations in V_{OC}, as summarized in Table 2.

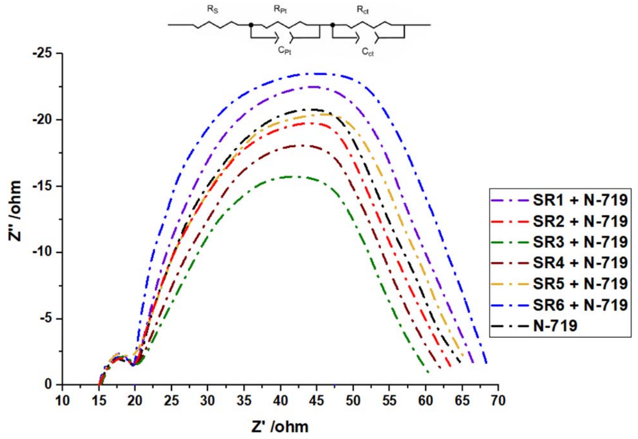

Fig. 12 Nyquist plots of **SR1–6** + **N719**-based devices.

4. Conclusion

This study provides a detailed investigation of phenothiazine-based sensitizers (**SR1–6**) for dye-sensitized solar cells (DSSCs), focusing on their spectral, electrochemical, and photovoltaic properties in both single-dye and co-sensitization configurations. While co-sensitization is an established approach in DSSCs, our findings offer new insights into how specific molecular structures influence device performance, particularly in enhancing light absorption, charge transfer dynamics, and interface stability. Among the single-dye devices, **SR1** demonstrated the highest efficiency (4.22%), followed by **SR6** (3.88%), emphasizing the importance of donor–acceptor interactions and energy level alignment. When co-sensitized with **N719**, **SR6** + **N719** achieved a notable efficiency of 9.77%, surpassing **N719**-only devices (7.33%). The electrochemical impedance spectroscopy (EIS), where **SR6** + **N719** exhibited the highest charge transfer resistance (R_{ct} = 49.98 Ω), indicating suppressed electron recombination and enhanced interfacial charge transport.

Consent to participate

All authors participated directly in the current research work.

Data availability

The data supporting this article have been included as part of the ESI.†

Conflicts of interest

Authors declare that they have no conflict of interest.

Acknowledgements

The authors are thankful to Academy of Scientific Research and Technology, Egypt, for their financial support under LEAP-RE, HORIZON program 2020.

References

1 M. K. Nazeeruddin, E. Baranoff and M. Grätzel, Dye-sensitized solar cells: A brief overview, *Sol. Energy*, 2011, **85**, 1172–1178.

2 C. Ballif, F. J. Haug, M. Boccard, P. J. Verlinden and G. Hahn, Status and perspectives of crystalline silicon photovoltaics in research and industry, *Nat. Rev. Mater.*, 2022, **7**, 597–616.

3 K. B. O'regan and M. Grätzel, A low-cost, high-efficiency solar cell based on dye-sensitized colloidal TiO_2 films, *Nat*, 1991, **353**, 737–740.

4 J. Gong, K. Sumathy, Q. Qiao and Z. Zhou, Review on dye-sensitized solar cells (DSSCs): Advanced techniques and research trends, *Renewable Sustainable Energy Rev.*, 2017, **68**, 234–246.

5 K. Prajapat, U. Mahajan, K. Sahu, M. Dhonde and P. M. Shirage, The Evolution of natural Dye-Sensitized solar Cells: Current Advances and outlook, *Sol. Energy*, 2024, **284**, 113081.

6 Z. Qbal, W. Q. Wu, Z. S. Huang, L. Wang, D. B. Kuang, H. Meier and D. Cao, Trilateral π-conjugation extensions of phenothiazine-based dyes enhance the photovoltaic performance of the dye-sensitized solar cells, *Dyes Pigm.*, 2016, **124**, 63–71.

7 D. Devadiga, M. Selvakumar, P. Shetty, M. Sridhar Santosh, R. S. Chandrabose and S. Karazhanov, Recent developments in metal-free organic sensitizers derived from carbazole, triphenylamine, and phenothiazine for dye-sensitized solar cells, *Int. J. Energy Res.*, 2021, **45**, 6584–6643.

8 H. Tian, X. Yang, R. Chen, Y. Pan, L. Li, A. Hagfeldt and L. Sun, Phenothiazine derivatives for efficient organic dye-sensitized solar cells, *Chem. Commun.*, 2007, **36**, 3741–3743.

9 H. H. Gao, X. Qian, W. Y. Chang, S. S. Wang, Y. Z. Zhu and J. Y. Zheng, Oligothiophene-linked D–π–A type phenothiazine dyes for dye-sensitized solar cells, *J. Power Sources*, 2016, **307**, 866–874.

10 I. M. Abdellah and A. El-Shafei, Efficiency enhancement of ruthenium-based DSSCs employing A–π–D–π–A organic Co-sensitizers, *RSC Adv.*, 2020, **10**(47), 27940–27953.

11 S. A. Badawy, E. Abdel-Latif, A. A. Fadda and M. R. Elmorsy, Synthesis of innovative triphenylamine-functionalized organic photosensitizers outperformed the benchmark dye N-719 for high-efficiency dye-sensitized solar cells, *Sci. Rep*, 2022, **12**(1), 12885.

12 M. Hoseinizadeh, K. E. Salem, A. Gouda, D. Belanger and C. Santato, Tannins for sustainable semi-solid-state supercapacitors, *Waste Biomass Valorization*, 2023, **14**(10), 3475–3488.

13 I. Althagafi and N. El-Metwaly, Enhancement of dye-sensitized solar cell efficiency through co-sensitization of thiophene-based organic compounds and metal-based, *Arab. J. Chem.*, 2021, **14**(4), 103080.

14 M. R. Elmorsy, F. H. Abdelhamed, S. A. Badawy, E. Abdel-Latif, A. A. Abdel-Shafi and M. A. Ismail, Design, synthesis, and performance evaluation of TiO_2-dye sensitized solar cells using 2, 2′-bithiophene-based co-sensitizers, *Sci. Rep.*, 2023, **13**(1), 13825.

15 H. M. El-Shafeai, S. A. Badawy, M. A. Ismail, E. Abdel-Latif, A. A. Fadda and M. R. Elmorsy, Synthesis of efficient bi-anchoring bifuran/biphenyl derivatives for dye-sensitized solar cell applications, *RSC Adv.*, 2023, **13**(14), 9720–9731.

16 C. H. Chen, Z. H. Luo, I. H. Huan, Y. H. Chen and T. S. Lim, Rationalize the roles of electron donating-withdrawing groups in the impacts on solvatochromism, nonlinear optics, and electroluminescence devices, *Dyes Pigm.*, 2020, **175**, 108143.

17 S. A. Badawy, E. Abdel-Latif and M. R. Elmorsy, Tandem dye-sensitized solar cells achieve 12.89% efficiency using novel organic sensitizers, *Sci. Rep.*, 2024, **14**(1), 26072.

18 M. R. Elmorsy, S. A. Badawy, H. S. Elmetwaly, E. H. Elrewiny, F. M. Eshra, A. E. Soliman, K. E. Salem, E. Abdel-Latif and M. M. Elkholy, Carbazole-phenothiazine sensitizers boost tandem DSSC efficiency to 12.85%, *Dyes Pigm.*, 2025, **233**, 112540.

19 S. A. Badawy, K. E. Salem, A. A. Fadda, E. Abdel-Latif and M. R. Elmorsy, Advancements in metal-free organic dyes: Achieving over 10% efficiency in DSSCs, *Dyes Pigm.*, 2024, **225**, 112096.

20 X. Chen, *et al.*, Electronic coupling mechanisms in dye-sensitized solar cells, *J. Phys. Chem. C*, 2022, **126**, 15678–15689.

21 K. Lee, *et al.*, Surface binding modes of organic sensitizers on TiO_2, *ACS Appl. Mater. Interfaces*, 2023, **15**, 23456–23467.

22 J. Park, *et al.*, *J*-aggregate formation in donor-π-acceptor dyes, *Adv. Energy Mater.*, 2021, **11**, 2100123.

23 H. Kim, *et al.*, Raman spectroscopic studies of dye aggregation, *Chem. Sci.*, 2022, **13**, 3456–3467.

24 M. Zhang, *et al.*, Energy level engineering in DSSCs, *Adv. Funct. Mater.*, 2022, **32**, 2100789.

25 J. Li, *et al.*, Interfacial electron transfer dynamics in DSSCs, *ACS Energy Lett.*, 2023, **8**, 1234–1245.

26 Y. Wu, *et al.*, Co-sensitization strategies for DSSCs, *Energy Environ. Sci.*, 2022, **15**, 3456–3467.

27 X. Sun, *et al.*, Molecular engineering of organic sensitizers, *Chem. Rev.*, 2023, **123**, 4567–4578.

28 H. Wang, *et al.*, Design principles for DSSC sensitizers, *Adv. Mater.*, 2023, **35**, 2200123.

29 S. Lee, *et al.*, Electronic processes in co-sensitized DSSCs, *Sci. Rep. Rep*, 2022, **12**, 3456–3467.

30 Y. Chen, *et al.*, Interfacial engineering in DSSCs, *Adv. Energy Mater.*, 2023, **13**, 2200456.

31 S. E. Mahmoud, A. A. Fadda, E. Abdel-Latif, *et al.*, Synthesis of Novel Triphenylamine-Based Organic Dyes with Dual Anchors for Efficient Dye-Sensitized Solar Cells, *Nanoscale Res. Lett.*, 2022, **17**, 71, DOI: 10.1186/s11671-022-03711-6.

32 M. A. M. Rashid, D. Hayati, K. Kwak and J. Hong, Theoretical investigation of azobenzene-based photochromic dyes for dye-sensitized solar cells, *Nanomater*, 2020, **10**, 914.

33 L. Zhang, *et al.*, Time-resolved spectroscopy of DSSCs, *Chem. Soc. Rev.*, 2022, **51**, 4567–4578.

34 J. Liu, *et al.*, Charge recombination in DSSCs, *J. Mater. Chem. C*, 2023, **11**, 5678–5689.

35 K. Park, *et al.*, Surface photovoltage spectroscopy of DSSCs, *ACS Appl. Energy Mater.*, 2022, **5**, 6789–6800.

36 S. Zhang, *et al.*, Molecular Engineering of Organic Sensitizers for Solar Cell Applications, *Chem. Commun.*, 2009, 2198–2200.

37 Z. Wu, *et al.*, Electron transfer dynamics in DSSCs, *Adv. Sci.*, 2022, **9**, 2100789.

38 M. K. Nazeeruddin, *et al.*, Sequential Co-Sensitization of TiO_2 Particulate Films by Ruthenium Dyes for Enhanced Light Harvesting in Dye-Sensitized Solar Cells, *J. Am. Chem. Soc.*, 2011, **133**, 3115–3123.

39 A. Yella, *et al.*, Porphyrin-Sensitized Solar Cells with Cobalt (II/III)–Based Redox Electrolyte Exceed 12% Efficiency, *Sci. Rep.*, 2012, **334**, 629–634.

40 M. Wang, *et al.*, An Organic Redox Electrolyte to Rival Triiodide/Iodide in Dye-Sensitized Solar Cells, *Nat. Chem.*, 2012, **2**, 385–389.

41 A. Mishra, *et al.*, Metal-Free Organic Dyes for Dye-Sensitized Solar Cells: From Structure: Property Relationships to Design Rules, *Angew. Chem., Int. Ed.*, 2009, **48**, 2474–2499.

42 L. Zhang, *et al.*, Ruthenium Sensitizer with p-Conjugated π-Extension for Dye-Sensitized Solar Cells, *Chem. Commun.*, 2012, **48**, 11685–11687.

43 A. Hagfeldt, *et al.*, Dye-Sensitized Solar Cells, *Chem. Rev.*, 2010, **110**, 6595–6663.

44 Q. Yu, *et al.*, High-Efficiency Dye-Sensitized Solar Cells: The Influence of Lithium Ions on Exciton Dissociation, Charge Recombination, and Surface States, *ACS Nano*, 2012, **6**, 961–970.

45 P. Wang, *et al.*, Enhanced Light-Harvesting in Dye-Sensitized Solar Cells with Highly Conjugated Zinc Phthalocyanine Sensitizers, *Energy Environ. Sci.*, 2010, **3**, 635–643.

46 Y. Chiba, *et al.*, Dye-Sensitized Solar Cells with Conversion Efficiency of 11.1%, *Jpn. J. Appl. Phys.*, 2006, **45**, 638–640.

47 F. Fabregat-Santiago, J. Bisquert, G. Garcia-Belmonte, G. Boschloo and A. Hagfeldt, Influence of electrolyte in transport and recombination in dye-sensitized solar cells studied by impedance spectroscopy, *Sol. Energy Mater. Sol. Cells*, 2005, **87**, 117–131.

48 F. Li, Y. Chen, X. Zong, W. Qiao, H. Fan, M. Liang and S. Xue, New benzothiadiazole- based dyes incorporating dithieno [3,2-b:2′,3′-d]pyrrole (DTP) π-linker for dye- sensitized solar cells with different electrolytes, *J. Power Sources*, 2016, **332**, 345–354.

49 M. Chen, L.-L. Shao, Y.-X. Guo and X.-Q. Cao, Nitrogen and phosphorus co-doped carbon nanosheets as efficient counter electrodes of dye-sensitized solar cells, *Chem. Eng. J.*, 2016, **304**, 303–312.

50 M. Chen, L.-L. Shao, Z.-Y. Yuan, Q.-S. Jing, K.-J. Huang, Z.-Y. Huang, X.-H. Zhao and G.-D. Zou, General strategy for controlled synthesis of NixPy/carbon and its evaluation as a counter electrode material in dye-sensitized solar cells, *ACS Appl. Mater. Interfaces*, 2017, **9**, 17949–17960.

51 L. Han, A. Islam, H. Chen, C. Malapaka, B. Chiranjeevi, S. Zhang, X. Yang and M. Yanagida, High-efficiency dye-sensitized solar cell with a novel co-adsorbent, *Energy Environ. Sci.*, 2012, **5**, 6057–6060.

52 J. Luo, Z. Wan, C. Jia, Y. Wang and X. Wu, A co-sensitized approach to efficiently fill the absorption valley, avoid dye aggregation and reduce the charge recombination, *Electrochim. Acta*, 2016, **215**, 506–514.

53 J. Luo, Z. Wan, C. Jia, Y. Wang and X. Wu, Co-sensitization of dithiafulvenyl-phenothiazine based organic dyes with N-719 for efficient dye-sensitized solar cells, *Electrochim. Acta*, 2016, **211**, 364–374.